



Full Text View

[Volume 32, Issue 10 \(October 2002\)](#)

Journal of Physical Oceanography

Article: pp. 2816–2827 | [Abstract](#) | [PDF \(1.46M\)](#)

Changes to Indian Ocean Subantarctic Mode Water in a Coupled Climate Model as CO₂ Forcing Increases

Helene Banks, Richard Wood, and Jonathan Gregory

Hadley Centre for Climate Prediction and Research, Met Office, Bracknell, Berkshire, United Kingdom

(Manuscript received April 16, 2001, in final form March 12, 2002)

DOI: 10.1175/1520-0485(2002)032<2816:CTIOSM>2.0.CO;2

ABSTRACT

Subantarctic mode water (SAMW) has been shown to be a good indicator of anthropogenic climate change in coupled climate models. SAMW in a coupled climate model and the response of modeled SAMW to increasing CO₂ are examined in detail. How SAMW adjusts from climatological values toward a new equilibrium in the coupled model, with different climatological temperature and salinity properties, is shown. The combined formation rate of SAMW and Antarctic intermediate water is calculated as approximately 18 Sv (Sv ≡ 10⁶ m³ s⁻¹) in the Indian sector of the Southern Ocean, slightly lower than climatological values would suggest. When forced with increasing CO₂, SAMW is produced at a similar rate but at lower densities. This result suggests that the rate of heat uptake in this part of the ocean will be unchanged by anthropogenic forcing. The important signal in the response of SAMW is the shift to colder and fresher values on isopycnals that is believed to be related to changes in thermodynamic surface forcing. It is shown that, given uniform forcing, SAMW is expected to enhance the signal relative to other water masses. Independent increases in surface heating or freshwater forcing can produce changes similar to those observed, but the two different types of forcing are distinguishable using separate forcing experiments, hodographs, and passive anomaly tracers. The changes in SAMW forced by increasing CO₂ are dominated by surface heating, but changes to freshwater fluxes are also important.

Table of Contents:

- [Introduction](#)
- [The coupled model and SAMW in the control simulation](#)
- [Changes as CO₂ increases](#)
- [What drives the changes](#)
- [Discussion](#)
- [REFERENCES](#)
- [TABLES](#)
- [FIGURES](#)

Options:

- [Create Reference](#)
- [Email this Article](#)
- [Add to MyArchive](#)
- [Search AMS Glossary](#)

Search CrossRef for:

- [Articles Citing This Article](#)

Search Google Scholar for:

- [Helene Banks](#)
- [Richard Wood](#)
- [Jonathan Gregory](#)

Subantarctic mode water (SAMW) is formed in large quantities in the Southern Ocean ([McCartney 1977](#)) and is indeed one of the most abundant water masses in the world oceans. SAMW can be identified by its minimum in the absolute potential vorticity ([McCartney 1977](#)) or alternatively by the maximum separation of isopycnals (which is commonly referred to as thickness). SAMW can form through convective mixing in wintertime, and the extreme thickness is believed to be the signature of the deep winter mixed layer.

Observations from the 1960s to the present day show that SAMW has cooled and freshened significantly on isopycnals ([Johnson and Orsi 1997](#); [Wong et al. 1999](#); [Bindoff and McDougall 2000](#)). This change is believed to be associated with a warming or freshening of surface waters ([Church et al. 1991](#)) and is attributed to a change in surface thermodynamic forcing ([Wong et al. 1999](#)), either with increased surface heat fluxes or increased precipitation at high latitudes (which is usually related to the first by an increased strength of the hydrological cycle; [Cubasch and Meehl 2001](#)). [Banks et al. \(2000\)](#) found that SAMW underwent a similar cooling and freshening on isopycnals in a coupled climate simulation with anthropogenic forcing. Furthermore, they showed that SAMW is a water mass with a high signal-to-noise ratio under anthropogenic forcing, especially in the Indian Ocean (rather than Pacific Ocean) sector. They hypothesize that the high sensitivity of SAMW may be partly due to the fact that it is a homogeneous water mass occupying a large volume.

Detection of climate change has been based traditionally on surface temperatures (e.g., [Barnett et al. 1999](#)); [Levitus et al. \(2001\)](#) and [Barnett et al. \(2001\)](#) more recently have examined model simulations to see whether they can reproduce the observed signal in ocean heat content ([Levitus et al. 2000](#)). The attraction of using watermass properties to detect change is that they can act to integrate changes in surface fluxes and hence they have a relatively low noise level. By contrast, surface fluxes themselves are highly variable and are difficult to derive, and therefore it would be much harder to detect long-term change. Given the potential importance of SAMW as a tool for detecting climate change, it is important to understand how well SAMW is represented in models and why changes occur under increasing greenhouse gases. The purpose of this paper is to examine SAMW in the coupled climate model used by [Banks et al. \(2000\)](#) in more detail. First, we will describe the model and experimental design ([section 2](#)) and the mean state of the modeled SAMW water mass as compared with observations: its formation rates, distribution, and properties ([section 3](#)). Second, we will describe how SAMW changes under anthropogenic forcing ([section 4](#)) and will explain why it changes ([section 5](#)). We will limit ourselves in this discussion to the Indian Ocean sector of the Southern Ocean, because that is where the climate signal is believed to be strongest.

2. The coupled model and experimental design

The model studied here is the Third Hadley Centre Coupled Ocean–Atmosphere General Circulation Model (HadCM3) described in some detail by [Gordon et al. \(2000\)](#). The control simulation (CTL) was initialized from rest with potential temperature and salinity values given by [Levitus and Boyer \(1994\)](#). In CTL, the atmospheric composition is that of 1860 with the partial pressure of carbon dioxide ($p\text{CO}_2$) equal to 290 ppm by volume. The control is not a simulation of present-day conditions, but the simulated climate changes that we discuss in the following sections are much larger than the differences between the climates of 1860 and present day. Moreover, as discussed by [Gordon et al. \(2000\)](#), the errors in the control simulation (at least for sea surface temperature) are also larger than the climate change between present day and 1860. The model water masses generally drift away from their initial climatological values and reach a new equilibrium after about 400 years. This can be seen by the fact that the actual transport of freshwater by the ocean does not initially balance the transport implied by the surface freshwater fluxes (this is a local imbalance because on a global basis the imbalance is small). The ocean adjusts until the actual and implied transports balance by rearranging the distribution of ocean salinity ([Pardaens et al. 2001](#), manuscript submitted to *Climate Dyn.*, hereinafter PAR). An approximate balance is reached after 400 years, and, although the ocean will continue to adjust on longer timescales, in a large-scale sense this is an important timescale. We will describe the adjustment of SAMW toward its equilibrium along with its properties after adjustment in the next section.

We will then look at changes in SAMW in an experiment with CO_2 increasing at a rate of 2% per year. We will call this experiment 2PC. This experiment was initialized from year 801 of CTL. [Banks et al. \(2000\)](#) discussed results from experiment B2 [which was based on an Intergovernmental Panel on Climate Change (IPCC) scenario; [Johns et al. 2001](#)]. [Figure 1](#) shows that doubling of CO_2 occurs after 35 years in 2PC, whereas the forcing increased more slowly in the B2 experiment. Until present day, IPCC scenario B2 is identical to other IPCC scenarios such as IS92a. We chose to focus on 2PC in this paper rather than on experiment B2 because the larger CO_2 forcing means that it is easier to separate the response from natural variability. However, we have performed similar analyses on B2 and believe that the mechanisms are the same in both experiments. In addition, 2PC was also run from an initial state starting in year 100. Although the ocean is still adjusting toward an equilibrium state at year 100, the effect of increasing CO_2 is the same as the results described in more detail here, suggesting that the drifts in the control run have negligible influence on the simulated climate change.

To help to understand the processes occurring in 2PC, we included a ventilation tracer. This tracer was inserted into the surface between 60° and 35°S (the region corresponding to the deep winter mixed layer) at a constant rate of 1 unit per

year. The tracer was initialized to zero at the start of year 1 and year 31. In 2PC we also used two tracers, which we will call passive anomaly temperature (PAT) and passive anomaly salinity (PAS). These tracers are inserted at the surface at a rate that is equal to the corresponding anomalous surface fluxes of heat and freshwater in 2PC. The anomalous surface flux is diagnosed by calculating the difference between the instantaneous surface flux in 2PC and climatological values from CTL. PAT and PAS are defined to have units of temperature and salinity, respectively, with increases in the surface heat and freshwater fluxes into the ocean leading to positive values of PAT and negative values of PAS, respectively (the changes are in the direction we would expect changes in temperature and salinity to occur).

In addition to CTL and 2PC, we also performed two experiments with extra heating (EH) and extra freshwater forcing (EF) applied. These experiments were initialized at year 470 of CTL and were run for 10 years with constant CO_2 and with extra heat or freshwater applied in the region between 60° and 35°S . Experiments EF and EH have different start times in CTL to that of 2PC (year 470 as opposed to year 801). We do not believe that this will affect the results because (i) by year 470 the ocean has adjusted considerably and the state is similar to that of year 801 and (ii) EH and EF are intended to be sensitivity experiments to indicate the influence of extra heat or freshwater forcing and the results should be independent of the exact initial state.

The magnitude of the forcing applied in EH and EF is described in [Table 1](#). The forcing in EH and EF was deliberately chosen to be large relative to 2PC and CTL. The real use of EH and EF is to demonstrate clearly the effect of pure warming or pure freshening on the ocean and in addition to verify the hodograph method of [Bindoff and McDougall \(2000\)](#). The heat and freshwater forcing were prescribed such that the buoyancy forcing was the same in both cases. This implies that

$$Q = \frac{\alpha H}{\beta C_p S_0}, \quad (1)$$

where Q is the surface freshwater flux (precipitation minus evaporation), H is the surface heat flux into the ocean, α ($=-1/\rho\partial\rho/\partial\theta$) and β ($=1/\rho\partial\rho/\partial S$) are the thermal expansion and haline contraction coefficients, C_p is the specific heat capacity, and S_0 [$=35$ practical salinity units (psu)] is the constant salinity used to convert freshwater fluxes to a virtual salt flux in the model. The ratio $\alpha:\beta$ is variable, which is why there is a range in the freshwater forcing with equivalent buoyancy forcing to constant heat forcing.

3. SAMW in the control simulation

As we have already described, SAMW can be traced in the ocean interior by its potential vorticity (PV) signature, which is calculated as

$$\frac{f}{\rho_0} \frac{\partial \rho}{\partial z}, \quad (2)$$

where f is the Coriolis parameter and ρ is potential density, and depth z is positive downward.

[Figure 2a](#) shows a cross section at 32°S of PV from [Levitus and Boyer \(1994\)](#). We chose to look at the 32°S section because there are a number of hydrographic sections at this latitude (note that in subsequent parts of the analysis we address the ocean volume south of 35°S ; however, this small shift in latitude will not affect the results). In the climatological data, the absolute value of PV reaches a local minimum¹ of $-5 \times 10^{-11} \text{ m}^{-1} \text{ s}^{-1}$ at 90°E between 26.5 and 27.0 kg m^{-3} (equivalent to a depth of approximately 400 m as seen in [Fig. 3a](#)). This distribution is in broad agreement with the instantaneous picture presented by [Toole and Warren \(1993\)](#) but is considerably smoother (as we would expect). [Figure 2b](#) shows the same cross section from years 801–810 of CTL. The PV minimum reaches $-6 \times 10^{-11} \text{ m}^{-1} \text{ s}^{-1}$ in CTL. The minimum in CTL is at densities between 25.5 and 26.0 kg m^{-3} (equivalent to a depth of approximately 300 m as seen in [Fig. 3b](#)) and shallower than the climatological value). The volume of water with PV greater than $-6 \times 10^{-11} \text{ m}^{-1} \text{ s}^{-1}$ between 138 and 447 m and between 32° and 60°S is $0.72 \times 10^{15} \text{ m}^3$ in HadCM3 and $1.9 \times 10^{15} \text{ m}^3$ in the climatological data. In HadCM3, a volume of SAMW equivalent to that of the climatological situation is represented by PV greater than $-12 \times 10^{-11} \text{ m}^{-1} \text{ s}^{-1}$.

The lower density of SAMW in CTL is reflected in the temperature and salinity; the average temperature of SAMW at years 801–810 of CTL (defined by the PV minimum) is 12.5°C and the average salinity is 34.3 psu , which compares to climatological values of 10.5°C and 34.9 psu . [Figure 4](#) shows the salinity and PV fields changing over time to make this adjustment. The e -folding timescale for adjustment is approximately 400 years. After this time, the properties of SAMW

have undergone a significant adjustment toward their modeled values at years 801–810. Antarctic intermediate water (AAIW) adjusts on a similar timescale; it initially has a salinity minimum of 34.5 psu at densities of 27.1–27.5 kg m⁻³ and freshens and lightens to values of 34.0 psu and 26.2–26.7 kg m⁻³. This is the same timescale found by PAR to be required for the freshwater budgets of the atmosphere and ocean to balance, and we believe that the differences are related to the adjustment of the water mass to balance the model's freshwater budget.

[Figure 5](#) shows the freshwater divergence implied by the surface fluxes over the Indian Ocean sector of the Southern Ocean. The surface fluxes are reasonably constant and give an average freshwater input of 0.18 Sv (Sv ≡ 10⁶ m⁻³ s⁻¹) over the 1180-yr period. This is in good agreement with the estimate of 0.2 Sv by [Sloyan and Rintoul \(2001b\)](#). The freshwater input from the surface fluxes implies a divergence of freshwater by the ocean in a steady state. However, in a transient state, the implied and actual divergences will not balance, and this imbalance will lead to a drift in the subsurface salinity. [Figure 5](#) shows the drift in the subsurface salinity for the water column both above and below 1000 m. In the first 5 yr, the top 1000 m accumulates an excess of freshwater, which is the result of a deficit in the actual divergence of freshwater by the ocean. Given that the implied divergences from the surface fluxes are close to observed and the ocean salinity field was initialized with climatological data, this result suggests that the deficit in the divergence of freshwater by the ocean may be due to weaknesses in the modeled circulation. The ocean model balances the implied divergences over a period of time by adjusting the distribution of salinity. Over the 1180 yr, the convergence of freshwater in the top 1000 m gradually reduces while below 1000 m the ocean on average loses freshwater. The total drift in the water column reduces to zero after 400 yr.

Although the actual properties of SAMW in the coupled model are now offset from the observed values, the model signature in PV is subsequently maintained over 1000 years. [Figure 6](#) shows the deep winter mixed layer and the extent of the PV minimum at densities of 25.8–26.0 kg m⁻³. This shows SAMW as a tongue stretching northwestward from the formation zone in the winter mixed layer. This distribution was used by [McCartney \(1982\)](#) to infer the advection of mode water around the subtropical gyre. [Marsh et al. \(2000\)](#) confirmed this inference in an isopycnal ocean model by tracking particles from their sources. If we were to look for lighter modes, we would find them being formed to the west of this mode, and denser modes would be found to the east. Both lighter and denser modes show a similar propagation around the subtropical gyre.

We can also ask if the rates of production are correct. [Table 2](#) shows the volume transport in four density classes across the three sections marked in [Fig. 6](#) (with the sections at 21° and 120°E extending southward to 90°S). We have split the transport across each section into two components; the transport out of the sector and the transport into the sector. In the density class 25.6–26.4 kg m⁻³, which represents SAMW and the upper part of AAIW, there is a net transport of approximately 26 Sv eastward through the sector, driven by the Antarctic Circumpolar Current. Almost 27 Sv are transported northward across 32°S, with 24 Sv returning southward and 12 Sv leaving the sector westward through the Agulhas Current. The divergence of the transport gives the formation rates (in [Table 2](#) this is given by the sum of the transports out of the sector and those into the sector.) The modeled rate of combined SAMW and AAIW formation at densities between 25.6 and 26.4 kg m⁻³ is 14.8 Sv. This can be compared with the observational estimate of [Sloyan and Rintoul \(2001a\)](#). They examined the Indian Ocean sector of the Southern Ocean using sections similar to the three sections taken here. Their Fig. 10 gives an estimate of the formation rate of SAMW of 11.9 Sv and of AAIW of 1.9 Sv. Formation rates can also be calculated using the buoyancy forcing method ([Speer and Tziperman 1992](#)). We are interested in formation rates here, which are defined as

$$-\partial F/\partial \rho, \quad (3)$$

where $F(\rho)$ is the transformation rate, defined as

$$F(\rho) = \frac{1}{\Delta \rho} \frac{1}{\text{year}} \int_{\text{year}} dt \int_{\text{area}} dA \left(\frac{-\alpha H}{C_p} - \beta Q S_0 \right) \times \Pi \left[\left(\rho + \frac{\Delta \rho}{2} \right) - \left(\rho - \frac{\Delta \rho}{2} \right) \right], \quad (4)$$

where Π is equal to 1 within and 0 outside the range $\pm \Delta \rho/2$. Transformation can essentially be thought of as the volume flux to higher or lower densities due to surface forcing, whereas the formation rate is the convergence of volume into particular density classes. Here we take $\Delta \rho$ to be equal to 0.2 kg m⁻³. If we take a lower $\Delta \rho$, the transformation profile is relatively unchanged, but the formation profile (which is the derivative of the transformation) can become very noisy. This

result was also found by [Speer and Tziperman \(1992\)](#).

The calculation of formation rates for the Indian sector (between 32° and 90°S) is shown in [Fig. 7](#) and gives a formation rate of 17.6 Sv for years 801–810 in the density range of 25.6–26.4 kg m⁻³. The shaded region indicates the range of formation rates from the ten decades covering years 761–860, showing little variation in production of SAMW and AAIW. In the density range in which SAMW and AAIW are formed, the average formation rate over this period is 18.5 Sv, with a standard deviation of 0.6 Sv. This estimate of the formation rate via the surface buoyancy fluxes is in reasonable agreement with the estimate via the flux divergences, and the differences should be accounted for by diapycnal mixing ([Nurser et al. 1999](#)).

Using the Comprehensive Ocean–Atmosphere Dataset (COADS) data of [Da Silva et al. \(1994\)](#), [Speer et al. \(1997\)](#) calculated the formation rate of SAMW and upper AAIW (between neutral densities of 26.5 and 27.3 kg m⁻³) as approximately 25 Sv, and in an isopycnal ocean model forced by climatological values, [Marsh et al. \(2000\)](#) found that the formation rate was approximately 22 Sv. These results suggest that the formation in the coupled model may be too weak by between 2 and 7 Sv. However, there is reason to doubt the accuracy of climatological fluxes in the Southern Ocean, given the lack of observations in that region, and it would therefore be unwise to place too much weight on the difference in the magnitude of the formation rates.

4. Changes as CO₂ increases at 2% per year

In this section, we will examine how the properties and ventilation rates of SAMW change as CO₂ increases. We will generally focus on the decade of CTL considered earlier (years 801–810, which cover the same time period as the first decade of 2PC) and the fourth decade of 2PC (years 31–40) when doubling of CO₂ occurs. In many cases, we will focus on the September average of the decades (i.e., the average of 10 Septembers). This approach is because the mixed layer is at its deepest in September and we can focus on the signal in the ocean interior rather than confuse the signal with shallow summer mixed layers.

a. Ventilation


[Figure 8](#) shows meridional cross sections at 85°E. In CTL, low PV is confined between 25.8 and 26.0 kg m⁻³; in 2PC the lowest PV is between 25.6 and 25.8 kg m⁻³. This clearly shows that the core of SAMW has moved to lighter density classes and suggests that ventilation continues but at lower densities. When comparing changes in thickness between 2PC and CTL over 35-yr periods, we find that the average increase in absolute PV on the 25.9 kg m⁻³ density surface in 2PC exceeds the maximum increase in absolute PV in CTL over any 35-yr period after year 400 on the same density surface. This result suggests that the change in 2PC is significant and is highly unlikely to be due to internal variability.


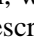
To look at this possibility further, we will compare the ventilation tracer (described in [section 2](#)) distributions for year 10 and year 40 of 2PC. The ventilation tracer is input to the surface at a constant rate, so the total tracer amount (integrated over the total volume) is the same for each of these years. However, changes in the tracer distribution can tell us about which density or depth classes are being ventilated. [Figure 9](#) shows the inventory (the area-averaged tracer amount on an isopycnal) for this tracer in density classes in the Indian Ocean. The total tracer amount is conserved when integrated globally, but this is not necessarily the case when considering only the Indian Ocean sector. [Figure 9](#) clearly shows that the tracer uptake has moved to lower densities, with the maximum in tracer uptake moving to a density that is 0.2 kg m⁻³ lighter. Because the tracer was inserted at a constant rate, it is not possible to use this result to determine whether formation rates for SAMW have changed. [Figure 7](#) shows the formation rates for years 31–40 of 2PC. Once again we see that the maximum formation has shifted to a density that is 0.2 kg m⁻³ lighter. The total production of SAMW is reduced slightly; in the density classes considered earlier (25.6–26.4 kg m⁻³), SAMW production is now 16.7 Sv.



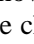

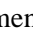
In general, this picture suggests that as the surface becomes lighter (from warming and salinity changes), ventilation of SAMW continues to take place in a similar geographical position, corresponding to a move to lower density classes. Previous work had suggested that decreasing PV at lower densities and increasing PV at high densities (as seen in [Fig. 8](#)) might indicate an increased production of SAMW at the expense of AAIW ([Banks et al. 2000](#); because decreasing PV indicates increased separation of density surfaces, this result might be interpreted as an increased volume of that particular water mass). However, the almost negligible change in formation rates suggests that the pattern of PV change should be interpreted as SAMW being formed at lower densities.


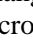

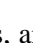
b. Temperature–salinity properties

[Bindoff and McDougall \(2000\)](#) observed that SAMW at 32°S cooled and freshened on isopycnals between 1962 and 1987. [Banks et al. \(2000\)](#) showed that, in a climate change experiment forced with historical greenhouse gases, changes that were both qualitatively and quantitatively similar occurred over the same time period.

In the process of forming, SAMW takes the θ - S properties of the winter mixed layer into the interior; the warmest and saltiest SAMW is the lightest form of SAMW and is found closest to the surface, whereas the coldest and freshest SAMW is the densest form of SAMW and is found at the deepest levels (just above AAIW). If these properties warm or freshen (as illustrated in [Figs. 10a,b](#) ) it will lead to cooling and freshening on isopycnals of the interior properties. [Banks et al. \(2000\)](#) looked at the changes over a 30-yr period in experiment B2 and found that the modeled cooling and freshening on isopycnals has a similar magnitude to the observations of [Bindoff and McDougall \(2000\)](#) but at a different density. However, in both cases, the largest change occurs in the mode waters and, as discussed in [section 3](#), the model mode water has shifted to a lower density over the adjustment period. Experiment 2PC at years 31–40 shows changes at 32°S similar to those seen in B2.

Observations are limited in their ability to describe the three-dimensional structure of changes, and the model can help to bridge this gap. [Figure 11a](#)  shows the zonally averaged salinity on level surfaces as a cross section through the Indian Ocean for years 801–810 of CTL. The salinity minimum associated with AAIW is highlighted. The minimum is at approximately 700 m in the model, which is 200–300 m shallower than observations suggest. This result is also likely to be a consequence of the model drift described in [section 3](#). [Figures 11b,c](#)  show the zonally averaged changes in temperature and salinity, respectively, on level surfaces between years 801–810 of CTL and years 31–40 of 2PC. We have restricted shading to areas in which the changes are greater than both the model drift and the variability on 30-yr timescales (as calculated from decadal means of years 761–860). As we might expect, the temperature of the water column has increased considerably in association with global warming. The exception to this increase in the southern Indian Ocean is a region from 0° to 30°S and extending from below 1500 up to 500 m, in which the ocean has cooled, although much of the cooling is not significant. The salinity changes are more complicated; there is a broad pattern of freshening which is largest in the southern Indian Ocean near the surface by the Antarctic continent and extends from the surface at 15°S to a depth of 400 m at 30°S, with the ocean becoming saltier around 45°S and close to the equator.

[Figure 12](#)  shows the same quantities as [Fig. 11](#)  but with differences calculated on density surfaces rather than level surfaces. The changes in temperature and salinity ([Figs. 12b,c](#) ) are now comparable in pattern (as they must be). There is a maximum cooling and freshening at 30°S between the 25 and 26 kg m⁻³ surfaces, with a magnitude of 0.4°C and 0.12 psu. Relative to [Fig. 11](#) , it can be seen that changes on density surfaces appear to be generally more significant relative to the internal variability than the changes on pressure surfaces. We expect that this is because we have eliminated changes due to the movement of density surfaces (commonly known as “heave”). [Figure 13](#)  shows the cooling on the 25.8–26.0 kg m⁻³ isopycnal. The cooling on this isopycnal exceeds 0.6°C, and there is an impression of the cooling originating in the source region and propagating away (e.g., see the 11.8°C contour). Comparing the changes in temperature–salinity (T - S) on density surfaces between 2PC and CTL, we find that the average cooling over 35 yr on the 25.9 kg m⁻³ isopycnal in 2PC exceeds 2 standard deviations of the 35-yr changes in CTL (from year 400 onward). Once again, this result suggests that the changes in 2PC are unlikely to be due to internal variability.


The three-dimensional picture presented shows that cooling and freshening on isopycnals originates at the source of SAMW and moves into the interior ocean. The fact that the cooling signal on isopycnals is strongest in the mode water is particularly striking in [Fig. 13](#) . In [Fig. 10](#) , we show that when the T - S curve is oriented parallel to isopycnal surfaces for the same warming or freshening (cf. [Figs. 10a](#)  with 10c and [Figs. 10b](#)  with 10d), the change along isopycnals is much larger than when the T - S curve does not lie almost parallel to isopycnals. The change in salinity on an isopycnal, S'_n , can be expressed mathematically for the warming case [Eq. (7) of [Bindoff and McDougall 1994](#)] as

$$S'_n = -\theta'_z (G - G_\rho)^{-1}, \quad (5)$$

where θ'_z is the change in potential temperature at a constant depth, G is the slope on the T - S diagram of the T - S characteristic (θ'_z/S'_z), and G_ρ is the slope of the isopycnal (β/α). The change on isopycnals is largest where $(G - G_\rho)$ is smallest.

As we have discussed previously, mode water is identified by low PV. Potential vorticity can be expressed as

$$\frac{f}{\rho_0} \frac{\partial \rho}{\partial z} = \frac{f}{\rho_0} \alpha S_z (G - G_\rho), \quad (6)$$

which shows that, although the quantity $(G - G_\rho)$ is related to PV, low PV does not imply low $(G - G_\rho)$. [Figure 3](#) 

shows regions of low $(G - G_\rho)$ superimposed on PV for Levitus climatological values (Fig. 3a) and HadCM3 (Fig. 3b), suggesting that, at least in practice, low PV and low $(G - G_\rho)$ are closely related. Of course, this may not be the case for other mode waters, so we do not expect this to be a general result. However, for uniform surface forcing in the Indian Ocean, we might expect the signal of change on isopycnals to be in approximately the same position as low PV (this is indeed the case when we compare Fig. 13c and Fig. 6). In the next section, we will look more closely at the forcing for these changes.

5. What drives the changes in SAMW?

The surface heat and freshwater flux both change in 2PC. The surface heat flux shows a pattern of mostly warming, with an average heat flux increase between 35° and 60°S of 3 W m^{-2} (see Table 1). The freshwater changes show increased precipitation in high latitudes (south of approximately 45°S) and in the subtropical gyre between 15° and 30°S, with increased evaporation between 30° and 45°S and near the equator. The average freshwater increase between 35° and 60°S is 23 mm yr^{-1} (see Table 1). Both of these changes could, in theory, cause the observed cooling and freshening on isopycnals.

The changes in the surface fluxes can be seen clearly in the passive anomaly tracers. PAT (Fig. 14a) shows that increased surface heating penetrates to depth in the southern Indian Ocean, which is in agreement with the general pattern of increased surface heat fluxes over the ocean. PAS (Fig. 14b) shows that increased precipitation is advected into the interior at high latitudes while in the subtropics increased evaporation is advected into the interior. At lower latitudes, the pattern of increased evaporation near to the equator and precipitation between 15° and 30°S is also in agreement with the changes in the surface freshwater fluxes described above. The difference between Fig. 11 and Fig. 14 (in particular between salinity and PAS) shows that the active tracer fields are affected by changes in ocean circulation in addition to surface fluxes. However, if pure heave (vertical movement of the density surfaces) explained the interior changes, then the concentrations of PAT and PAS would be approximately equal to 0, suggesting that heave is not a dominant mechanism.

Given that heave is not the dominant mechanism, we would like to be able to identify whether heat changes or freshwater changes are more important. Bindoff and McDougall (1994) suggested that it should be possible to distinguish warming, freshening, and heave by plotting two pieces of independent information from section average profiles. Here we use the same axes employed by Bindoff and McDougall (2000): $[R_\rho / (R_\rho - 1)]\beta\delta S$ and $1/(R_\rho - 1)\alpha\delta\theta$, where $R_\rho [= (\alpha\theta_z)/(\beta S_z)]$ is the stability ratio (which varies through the water column), and δS and $\delta\theta$ are the changes in temperature and salinity on level surfaces. Plotting these two variables should allow a distinction between the three processes: when pure warming occurs, δS is zero and changes lie parallel to the y axis; when pure freshening occurs, $\delta\theta$ is zero and changes lie parallel to the x axis; and when pure heave occurs, $\alpha\delta\theta$ is equal to $R_\rho\beta\delta S$ and changes lie parallel to the diagonal (Bindoff and McDougall 2000).

The hodograph method is underconstrained because with two pieces of information we cannot discriminate between three processes. However, the passive anomaly tracers suggest that heave is relatively unimportant, and therefore we may be able to distinguish between pure warming and pure freshening.

To explore the likely impact of a change in surface heating or freshwater on SAMW properties, in addition to 2PC we will look at experiments EH and EF (described in section 2). The sensitivity experiments were run for 10 yr and are compared with the parallel 10-yr mean from CTL. Both experiments produce cooling and freshening on isopycnals of SAMW (Fig. 15). Figure 16 shows the hodographs for the section averages of 32°S for the change in the two ideal experiments EH and EF (relative to the parallel period in CTL) and for the change between years 31–40 of 2PC and years 801–810 from CTL. In each case, we have plotted the hodograph with lines denoting warming (W), freshening (F), and heave (H). In addition, we have also marked a line (E) to denote equal buoyancy forcing by heat and freshwater. This line is based on the fact that, for equal buoyancy forcing, $\alpha\delta\theta$ is equal to $-\beta\delta S$ and changes will lie along the line $x = -R_\rho y$. In SAMW, R_ρ lies between 20 and 3, and we have used the lower limit to denote the equal forcing.

The hodograph for EF (Fig. 16b) shows that changes near the surface are caused by freshening (due to the enforced increase in precipitation) while at depth any changes are very small. The hodograph for EH (Fig. 16a) is more difficult to interpret; near the surface, it appears that salinification is driving changes, at middepths heating is responsible, and at depth the changes are again small. It is presumed that enforcing surface heating feeds back on the freshwater cycle and drives increased evaporation from the surface. Do these results help us to interpret the results from 2PC? Run 2PC (Fig. 16c) shows a combination of all forcings: increased evaporation at the surface, changes at middepth driven by increased heating, changes below middepth caused by increased precipitation, and small changes at depth. Most of the crosses lie above the equal buoyancy forcing line, showing that in most cases heating is the dominant factor in SAMW. This interpretation agrees with the changes in the surface fluxes as seen in Fig. 14: the freshwater flux decreases at the surface at 32°S, some of the largest increases in the heat flux occur in the ventilation region for SAMW, and the freshwater flux increases at higher latitudes at which AAIW is formed.

6. Discussion

In this paper, we have examined Subantarctic mode water in the Indian Ocean sector of the Southern Ocean in the coupled model HadCM3. In the control experiment, SAMW adjusts over a 400-yr period until it reaches a new equilibrium. SAMW and upper Antarctic intermediate water form at a rate of approximately 18 Sv per year, which is slightly less than studies with climatological forcing have suggested, and the mode water is found to be approximately 1 kg m^{-3} lighter than climatological values such as those of [Levitus and Boyer \(1994\)](#).

We have looked in detail at the response of SAMW to increasing CO_2 in the atmosphere. The results show that the volume production of SAMW is unchanged as CO_2 increases at a rate of 2% per year until doubling of CO_2 occurs but that production moves to densities 0.2 kg m^{-3} lighter. This leads to ventilation on a particular isopycnal moving eastward. Increasing CO_2 in the atmosphere leads to increased surface heating of the ocean and a change to the freshwater cycle, with increased precipitation at high latitudes and increased evaporation in the subtropics. All three changes are responsible for driving changes in watermass properties at 30°S in the Indian Ocean.

We have shown that we expect ventilation to move to lower densities in response to anthropogenic climate change but with a similar production rate. Because production rates do not change, we expect the ocean to take up anthropogenic heating at a similar rate to present day in the future (at least for the part of the ocean considered here). Using the passive anomaly temperature, we can quantify the uptake of heat by SAMW in the Indian Ocean as 0.03 W m^{-2} as compared with 0.48 W m^{-2} for the global ocean below the mixed layer. This fraction may seem small, but SAMW represents just 0.5% of the volume yet is taking up 6% of the heat, implying that it is a highly efficient water mass.

[Banks et al. \(2000\)](#) inferred from a coupled model that SAMW was a good indicator of anthropogenic climate change. By showing that SAMW has a reasonably realistic production rate and distribution in the same coupled model, we strengthen that result. The anthropogenic signal of cooling and freshening on isopycnals is largest in mode waters, and we have shown that this result is partly because in SAMW T - S curves lie almost parallel to isopycnals, leading to an enhanced signal, even with uniform surface forcing. This result, in particular, gives a physical reasoning for the claim that one of the best places to observe anthropogenic climate change is in SAMW. Last, we have shown that in the coupled model the response of SAMW to anthropogenic climate change is dominated by changes to heat fluxes but freshwater fluxes do play a role.

Acknowledgments

This work was carried out under DETR Contract PECD 7/12/37. We thank Dr. Trevor McDougall for encouraging us to calculate the hodographs while HTB was visiting CSIRO and for his comments, which helped us to understand why SAMW might show an enhanced signal. We also thank Drs. Anne Paradaens, Howard Cattle, and Lynne Talley and two reviewers for their comments, which helped to improve this manuscript.

REFERENCES

Banks H. T., R. A. Wood, J. M. Gregory, T. C. Johns, and G. S. Jones, 2000: Are observed decadal changes in intermediate water masses a signature of anthropogenic climate change? *Geophys. Res. Lett.*, **27**, 2961–2964. [Find this article online](#)

Barnett T. P., Coauthors, 1999: Detection and attribution of recent climate change: A status report. *Bull. Amer. Meteor. Soc.*, **80**, 2631–2659. [Find this article online](#)

Barnett T. P., D. W. Pierce, and R. Schnur, 2001: Detection of anthropogenic climate change in the world's oceans. *Science*, **292**, 270–274. [Find this article online](#)

Bindoff N. L., and T. J. McDougall, 1994: Diagnosing climate change and ocean ventilation using hydrographic data. *J. Phys. Oceanogr.*, **24**, 1137–1152. [Find this article online](#)

Bindoff N. L., 2000: Decadal changes along an Indian Ocean section at 32°S and their interpretation. *J. Phys. Oceanogr.*, **30**, 1207–1222. [Find this article online](#)

Church J. A., J. S. Godfrey, D. R. Jackett, and T. J. McDougall, 1991: A model of sea level rise caused by ocean thermal expansion. *J. Climate*, **4**, 438–456. [Find this article online](#)

Cubasch U., and G. Meehl, 2001: Global climate models—Projections. *Climate Change 2001: The Scientific Basis*, J. T. Houghton et al., Eds., Cambridge University Press, 881 pp.

Da Silva A. M., C. C. Young, and S. Levitus, 1994: *Algorithms and Procedures*. Vol. 1, *Atlas of Surface Marine Data 1994*, NOAA Atlas NESDIS 6, 83 pp.

Gordon C., C. Cooper, C. A. Senior, H. Banks, J. M. Gregory, T. C. Johns, J. F. B. Mitchell, and R. A. Wood, 2000: The simulation of SST, sea ice extents and ocean heat transports in a version of the Hadley Centre coupled model without flux adjustments. *Climate Dyn.*, **16**, 147–168. [Find this article online](#)

Johns T. C., Coauthors, 2001: Anthropogenic climate change for 1860 to 2100 simulated with the HadCM3 model under updated emissions scenarios. Hadley Centre Tech. Note 22, 60 pp.

Johnson G. C., and A. H. Orsi, 1997: Southwest Pacific Ocean water-mass changes between 1968/69 and 1990/91. *J. Climate*, **11**, 831–847. [Find this article online](#)

Levitus S., and T. P. Boyer, 1994: *Temperature*. Vol. 4, *World Ocean Atlas 1994*, NOAA Atlas NESDIS 4, 129 pp.

Levitus S., J. I. Antonov, T. P. Boyer, and C. Stephens, 2000: Warming of the world ocean. *Science*, **287**, 2225–2229. [Find this article online](#)

Levitus S., J. Wang, T. L. Delworth, K. W. Dixon, and A. J. Broccoli, 2001: Anthropogenic warming of the earth's climate system. *Science*, **292**, 267–270. [Find this article online](#)

Marsh R., A. J. G. Nurser, A. P. Megann, and A. L. New, 2000: Water mass transformation in the Southern Ocean of a global isopycnal coordinate GCM. *J. Phys. Oceanogr.*, **30**, 1013–1045. [Find this article online](#)

McCartney M. S., 1977: Subantarctic mode water. *Deep-Sea Res.*, **24**, 103–119, (Suppl.). [Find this article online](#)

McCartney M. S., 1982: The subtropical recirculation of mode waters. *J. Mar. Res.*, **40**, 427–464, (Suppl.). [Find this article online](#)

Nurser A. J. G., R. Marsh, and R. G. Williams, 1999: Diagnosing water mass formation from air–sea fluxes and surface mixing. *J. Phys. Oceanogr.*, **29**, 1468–1487. [Find this article online](#)

Sloyan B. M., and S. R. Rintoul, 2001a: Circulation, renewal, and modification of Antarctic mode and intermediate water. *J. Phys. Oceanogr.*, **31**, 1005–1030. [Find this article online](#)

Sloyan B. M., 2001b: The Southern Ocean limb of the global deep overturning circulation. *J. Phys. Oceanogr.*, **31**, 143–173. [Find this article online](#)

Speer K., and E. Tziperman, 1992: Rates of water mass formation in the North Atlantic Ocean. *J. Phys. Oceanogr.*, **22**, 93–104. [Find this article online](#)

Speer K., S. Rintoul, and B. Sloyan, 1997: Subantarctic mode water formation by air–sea fluxes. *International WOCE Newsletter*, No. 29, WOCE International Project Office, Southampton, United Kingdom, 29–31.

Toole J. M., and B. A. Warren, 1993: A hydrographic section across the subtropical south Indian Ocean. *Deep-Sea Res.*, **40A**, 1973–2019. [Find this article online](#)

Wong A. P. S., N. L. Bindoff, and J. A. Church, 1999: Large-scale freshening of intermediate waters in the Pacific and Indian Oceans. *Nature*, **400**, 440–443. [Find this article online](#)

Tables

TABLE 1. Area-averaged surface heat flux (W m^{-2}) and freshwater flux (mm y^{-1}) between 35° and 60°S in the Indian Ocean sector of the Southern Ocean

Expt	Heat flux	Freshwater flux
CTL: years 801–810	–15.2	251.5
2PC years 31–40 minus CTL years 801–810	2.6	22.8
Extra heat (EH)	10	—
Extra freshwater (EF)	—	171–715

[Click on thumbnail for full-sized image.](#)

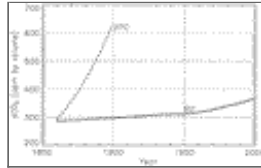
TABLE 2. Volume transport (Sv) across sections shown in Fig. 6 and resulting watermass formation (Sv) in density classes for years 801–810 of CTL for area bounded by 32°S , 21°E , and 120°E . Positive transport across a section indicates that it is out of

the area (i.e., northward across 32°S, westward across 21°E, and eastward across 120°E). Positive formation rates indicate that water mass is created in the area

Density class	32°S		21°E		120°E		Formation
	out	in	out	in	out	in	
$\sigma < 25.6$	15.16	-31.99	9.94	-1.66	0.52	0.0	-8.01
$25.6 < \sigma < 26.4$	20.99	-23.85	12.31	-20.10	31.15	-5.69	14.81
$26.4 < \sigma < 27.2$	12.75	-18.33	11.93	-66.22	66.22	-8.86	-0.51
$27.2 < \sigma$	6.61	-8.27	20.66	-187.94	165.96	-1.11	-6.29

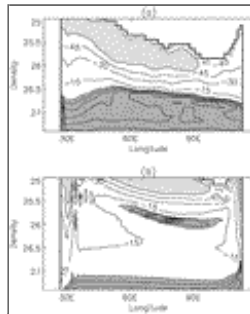
[Click on thumbnail for full-sized image.](#)

Figures



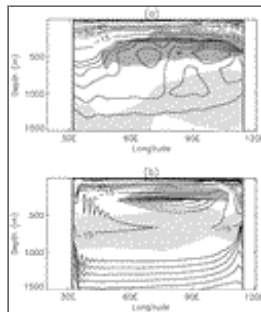
[Click on thumbnail for full-sized image.](#)

FIG. 1. The $p\text{CO}_2$ (ppm by volume) from experiment 2PC (this paper) and experiment B2 ([Banks et al. 2000](#))



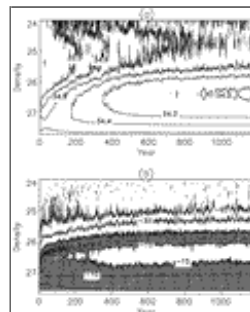
[Click on thumbnail for full-sized image.](#)

FIG. 2. Cross section of potential vorticity ($10^{-11} \text{ m}^{-1} \text{ s}^{-1}$) as a function of depth (density) across 32°S in the Indian Ocean from (a) climatological values and (b) years 801–810 from CTL. Light shading denotes regions with $PV < -60$; dark shading denotes regions with $PV > -10$ (contours within this region are at intervals of 1)



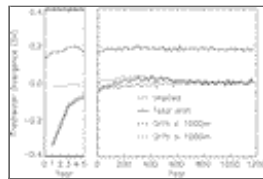
[Click on thumbnail for full-sized image.](#)

FIG. 3. Same as [Fig. 2](#), but depth is expressed in meters. The dark shading denotes areas where $|G - G_\rho|$ is less than 6. Light shading denotes areas where $|G - G_\rho|$ is greater than 20



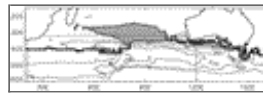
[Click on thumbnail for full-sized image.](#)

FIG. 4. Hovmöller diagrams of zonally averaged (a) salinity (psu) on isopycnals and (b) PV ($10^{-11} \text{ m}^{-1} \text{ s}^{-1}$) on isopycnals for



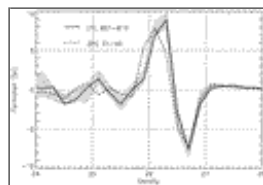
[Click on thumbnail for full-sized image.](#)

FIG. 5. Freshwater divergence implied by the surface fluxes and resulting divergence of freshwater in the Indian Ocean sector of the Southern Ocean due to a change in the salinity distribution for years 1–5 (based on annual means) and extended to year 1180 (based on decadal means)



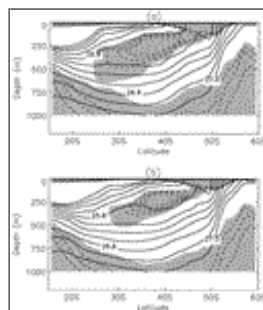
[Click on thumbnail for full-sized image.](#)

FIG. 6. Mixed layer depth in Sep for years 801–810 contoured for depths 150, 200, and 250 m. The region for which the absolute PV is less than $10 \times 10^{-11} \text{ m}^{-1} \text{ s}^{-1}$ for density layer $25.8\text{--}26.0 \text{ kg m}^{-3}$ is shaded, with the thick line between 35° and 40°S indicating the position of the outcrop. Also shown with dots are the sections used for calculating volume transports



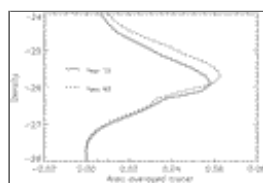
[Click on thumbnail for full-sized image.](#)

FIG. 7. Formation due to air–sea fluxes in the Indian sector for years 801–810 as a function of density. The method is described by [Speer and Tziperman \(1992\)](#). Shading indicates the range of formation from the period of 761–860. Also shown is the formation distribution for years 31–40 of 2PC



[Click on thumbnail for full-sized image.](#)

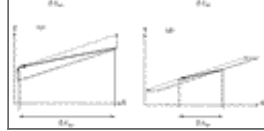
FIG. 8. Cross section of potential vorticity at 85°E . Shaded values indicate that the PV is less than $13 \times 10^{-11} \text{ m}^{-1} \text{ s}^{-1}$. Dashed contours inside the shaded region are at -10 , -8 , and $-6 \times 10^{-11} \text{ m}^{-1} \text{ s}^{-1}$. The bold contours are the density contours (at intervals of 0.2 kg m^{-3}) averaged over the same region



[Click on thumbnail for full-sized image.](#)

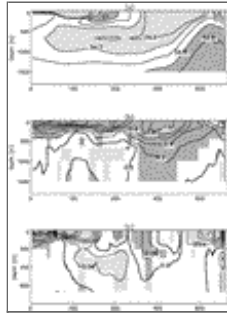
FIG. 9. Inventory of ventilation tracer in Indian Ocean on density surfaces from 2PC. Tracer is applied at a constant rate to the surface between 35° and 60°S initialized to zero at year 1 and year 31





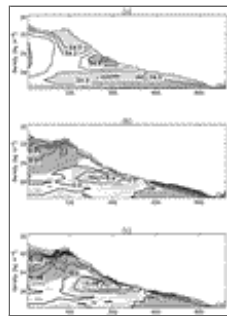
Click on thumbnail for full-sized image.

FIG. 10. The effect on the T - S curve if warming or freshening occurs: (a) warming and (b) freshening with a typical T - S curve. The T - S curve and an isopycnal are marked. The implied freshening along an isopycnal is denoted by ΔS_{1so} . (c) Warming and (d) freshening with T - S curves that are more parallel to the isopycnals and therefore are more representative of mode waters (where the density gradient is close to zero). The warming and freshening applied in (c) and (d) is the same as in (a) and (b), but ΔS_{1so} is much larger



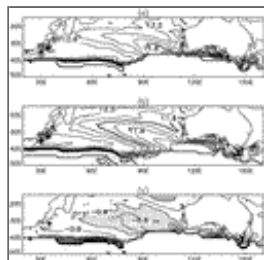
Click on thumbnail for full-sized image.

FIG. 11. (a) Zonally averaged salinity for the Indian basin for Sep average of CTL years 801–810 (light shading indicates values less than 34.2 psu; dark shading indicates values greater than 34.6 psu), (b) temperature change on level surfaces for Sep average of 2PC years 31–40 minus CTL years 801–810 (light shading indicates cooling; dark shading indicates warming), and (c) salinity change on level surfaces for Sep average of 2PC years 31–40 minus CTL years 801–810 (light shading indicates fresher water; dark shading indicates saltier water). Note that (c) is restricted to the top 700 m and the contour interval is 0.04 psu. In (b) and (c), only values that exceed model drift and variability on 30-yr timescales are shaded



Click on thumbnail for full-sized image.

FIG. 12. As in [Fig. 11](#) but on isopycnal surfaces



Click on thumbnail for full-sized image.

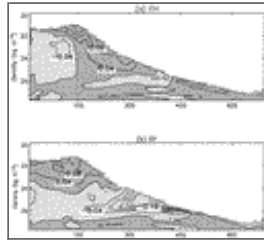
FIG. 13. Temperature of 25.8 – 26.0 kg m^{-3} isopycnal for (a) Sep average of CTL years 801–810 and (b) Sep average of 2PC years 31–40. Note the 11.8°C contour in bold. (c) The temperature of 2PC years 31–40 minus the temperature of CTL years 801–810 with light shading denoting cooling $>0.4^\circ\text{C}$ and dark shading denoting warming





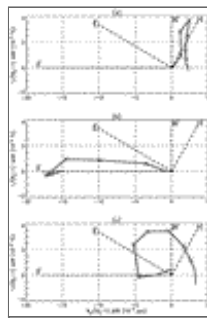
Click on thumbnail for full-sized image.

FIG. 14. (a) Zonally averaged passive anomaly temperature (light shading indicates cooling) and (b) zonally averaged passive anomaly salinity (light shading indicates freshening) for the Indian basin Sep average of 2PC years 31–40



Click on thumbnail for full-sized image.

FIG. 15. Change in salinity (psu) on isopycnals for (a) experiment with extra heating and (b) experiment with extra freshwater. The change is calculated as the decadal average from the sensitivity experiment minus the parallel period from CTL. Light shading denotes freshening



Click on thumbnail for full-sized image.

FIG. 16. Hodographs for the section averages across 32°S showing the results from experiments (a) EH, (b) EF, and (c) 2PC. In each case, the deepest levels are the end points that lie close to the origin. The points marked with a cross denote the model grid points that have density values between 25.0 and 26.2 kg m⁻³. The dashed lines W, F, H, and E denote warming, freshening, heave, and equal buoyancy forcing, respectively

Corresponding author address: Helene T. Banks, Hadley Centre for Climate Prediction and Research, Met Office, London Road, Bracknell, Berkshire RG12 2SY, United Kingdom. E-mail: helene.banks@metoffice.com

¹ Hereinafter we will simply refer to PV values closest to zero as “PV minimum,” meaning a minimum in absolute magnitude, noting that in the Southern Hemisphere PV is negative for a stable stratification.

top ▲

